Materials Advances

ROYAL SOCIETY OF CHEMISTRY

PAPER

View Article Online
View Journal | View Issue

Cite this: *Mater. Adv.*, 2026, 7, 2803

Unveiling the adsorption and electronic interactions of drugs on 2D graphsene: insights from DFT and machine learning approaches

Chaithanya Purushottam Bhat, Pranav Suryawanshi, Aditya Guneja and Debashis Bandyopadhyay *

Received 27th December 2025,
Accepted 22nd January 2026

DOI: 10.1039/d5ma01519g

rsc.li/materials-advances

Efficient identification of promising drug candidates for nanomaterial-based delivery systems is essential for advancing next-generation therapeutics. In this work, we present a synergistic framework combining density functional theory (DFT) and machine learning (ML) to explore the adsorption behavior and electronic interactions of drugs on a novel 2D graphene allotrope, termed graphsene (GrS). Graphsene, characterized by its porous ring topology and large surface area, offers an excellent platform for efficient adsorption and strong electronic coupling with drug molecules. A dataset comprising 67 pairs of different drugs adsorbed on various 2D substrates was employed to train the ML model, which was subsequently applied to predict suitable drug candidates for GrS based on molecular size and adsorption energy criteria (a database link is provided in a later section). The ML model exhibited robust predictive accuracy, achieving a mean absolute error of 0.075 eV upon DFT validation, though its sensitivity to initialization highlighted the need for larger and more diverse datasets. DFT-based analyses, including adsorption energetics, projected density of states (PDOS), and Bader charge calculations, revealed pronounced charge transfer and electronic coupling between the drug molecules and the GrS surface, elucidating the fundamental nature of drug–substrate interactions. This study reveals that the integrated DFT-ML strategy offers a rapid, cost-efficient approach for screening and understanding drug–nanomaterial interactions, paving the way for data-driven design of advanced nanomaterial-enabled drug delivery systems.

1. Introduction

The development of advanced materials for drug delivery has emerged as a rapidly growing field at the intersection of nanotechnology and biomedicine, providing innovative strategies for precise therapeutic delivery and enhanced clinical performance.[1,2] Conventional drug delivery systems often suffer from limitations such as low bioavailability, poor targeting efficiency, and uncontrolled release rates, which reduce therapeutic effectiveness and increase side effects. In this context, the exploration of two-dimensional (2D) nanomaterials offers a transformative approach due to their unique structural and physicochemical characteristics. Since the discovery of graphene, there has been a surge of research directed toward newly synthesized 2D materials with tunable surface properties, exceptional mechanical strength, and chemical versatility.[3,4] These materials provide ultrathin architectures with large surface-to-volume ratios, which can accommodate a variety of drug molecules through noncovalent adsorption, electrostatic interaction, or chemical functionalization. Their high chemical stability ensures the integrity of the carrier under physiological conditions, while adjustable electronic and surface properties allow for modulation of drug–substrate interactions and controlled drug release profiles. Consequently, the rational design and characterization of novel 2D nanomaterials hold great promise for creating next-generation, high-performance drug delivery systems capable of targeted, efficient, and sustained therapeutic action.[5–8]

Graphsene (GrS), a newly reported graphene allotrope,[9–11] is a carbon-based monolayer composed of fused tetra-, penta-, and dodeca carbon rings. This unique structural arrangement introduces significant porosity and anisotropy, distinguishing GrS from conventional graphene. Such characteristics make it a promising material for drug delivery applications, as the high surface area and tunable surface chemistry enable efficient adsorption of drug molecules and controlled interaction with specific drug functionalities. The use of density functional theory (DFT) provides a powerful approach to evaluate the

Department of Physics, Birla Institute of Technology and Science Pilani, Pilani, Rajasthan – 333031, India. E-mail: bandy@pilani.bits-pilani.ac.in, Debashis.bandy@gmail.com

suitability of GrS for drug delivery prior to experimental studies. Through DFT, one can precisely analyze adsorption energies, electronic structure modifications, and charge transfer processes at the atomic level, offering valuable insights for the rational design of GrS-based drug carrier systems. Nonetheless, large-scale DFT screening across numerous drug candidates remains computationally demanding, which can limit the pace of discovery and optimization in this emerging field.[12–14]

To overcome the computational challenges associated with large-scale DFT simulations, the integration of machine learning (ML) offers a powerful alternative for the design and optimization of 2D material-based drug delivery systems.[15,16] A deep learning framework can be developed to efficiently predict adsorption energies, charge transfer characteristics, and interaction mechanisms between 2D materials and various drug molecules.[17,18] By training these models on high-quality datasets obtained from representative DFT calculations, the ML approach can learn the underlying physical and chemical relationships governing molecular adsorption and electronic behavior. Once trained, such models are capable of rapidly estimating key interaction parameters for a wide range of drug–substrate combinations, drastically reducing the computational time required for exhaustive DFT-based evaluations. This enables the efficient screening of large chemical spaces and supports the rational selection of promising drug–material pairs.[19–23] Recent advances in ML, particularly graph neural networks (GNNs), have demonstrated exceptional ability to represent complex atomic structures and capture interatomic interactions with high accuracy. These models can interpret structural descriptors directly from atomic connectivity, making them especially suitable for predicting the adsorption and electronic properties of 2D materials.[24–27] By integrating ML predictions with first-principles DFT validation, the combined framework enhances both the speed and reliability of materials property prediction. This hybrid approach not only accelerates the identification of optimal 2D drug carriers like graphsene (GrS) but also deepens our understanding of the structure–property relationships governing adsorption behavior. Ultimately, the ML-assisted design pipeline opens new pathways for data-driven discovery and optimization of nanomaterials tailored for next-generation drug delivery applications.[28–32]

In the present study, we present an integrated machine learning (ML) and density functional theory (DFT) approach for the accelerated design of efficient two-dimensional (2D) drug delivery systems, focusing on the recently developed graphene allotrope, graphsene (GrS). The exceptional porosity, anisotropy, and tunable electronic features of GrS make it a promising platform for molecular adsorption and controlled drug release. To harness these properties effectively, ML models were trained on an adsorption energy dataset to predict the interaction affinities between a wide range of drug molecules and GrS-based substrates. The ML framework employs randomized initialization to ensure model robustness and comprehensive exploration of chemical space, enabling rapid identification of potential drug candidates with favorable binding characteristics. The most promising candidates, selected based on molecular compatibility, optimal adsorption energy, and functional suitability, were subsequently validated through DFT calculations to obtain precise adsorption geometries and energetics. Furthermore, projected density of states (PDOS) and Bader charge analyses were performed to examine the nature of electronic interactions and charge redistribution between the drug molecules and the GrS surface. This combined ML DFT methodology not only reduces the computational cost associated with conventional first-principles simulations but also provides a deeper understanding of the physicochemical mechanisms governing drug adsorption, offering a robust and data-driven pathway for the rational design of next-generation 2D nanomaterials for targeted drug delivery applications.

2. Methodology

The objective of this model is to predict the adsorption energy for drug–material pairs, which serves as a crucial parameter for assessing their suitability in drug delivery applications. Due to limited data availability, pre-training the model is necessary to achieve robust performance. To further optimize the model, five DFT results using graphene as the substrate were incorporated into the dataset for targeted fine-tuning. This approach leverages the unique properties of graphsene, such as its high surface area and biocompatibility, making it an ideal candidate for drug carrier design. Broadly, the model has two parts: a graph-based encoder and a multi-layer perceptron (MLP) as a decoder.

2.1. Dataset

In this study, two datasets were employed to carry out the integrated DFT machine learning analysis of drug adsorption on the novel 2D material, graphsene. The first dataset, QM9[33] (Quantum Machine 9), comprising over 10 000 drug-like molecules and 19 physicochemical properties, was utilized to pre-train the encoder network. The second dataset was constructed from previously reported studies on drug–material interactions, containing more than 60 pairs of 2D materials and drug molecules along with their corresponding adsorption energies. This combined data framework ensures both broad chemical diversity and specific adsorption information, enabling accurate modeling and prediction of drug–graphsene interactions.

2.1.1. Constructing molecular graphs. To represent the chemical and structural information of the systems, all drug molecules were encoded as molecular graphs, where atoms are treated as nodes and chemical bonds as edges. Each node was assigned a comprehensive feature vector that includes a one-hot encoding of the atom type along with key atomic descriptors such as atomic mass, formal charge, electronegativity, and coordination degree, thereby capturing both the elemental identity and topological environment. The molecular graphs were generated using the RDKit[34] library, which ensures efficient and accurate graph construction from molecular structures. It is important to note that these graphs represent the 2D connectivity of the molecules and do not explicitly encode

conformational (3D) information. For 2D materials, a slightly modified approach was implemented—atoms were defined as nodes and edges were established based on a distance cut-off criterion to identify neighboring atoms. Although this method can occasionally introduce additional or missing connections, it does not significantly affect the overall message-passing and learning performance of the graph-based model.

2.2. Model

To predict the adsorption energy (E_d) of drug molecules on graphsene, a graph convolutional network (GCN) framework was employed due to its proven capability in effectively learning representations from molecular graph structures. The model architecture consists of two parallel GCN encoders, each dedicated to processing the molecular graph of either the drug or the 2D material. For each graph, two types of pooled feature vectors, maximum pooling and mean pooling, were extracted to capture both the dominant and average structural characteristics. Consequently, four feature vectors (two from each GCN encoder) were obtained and concatenated to form a unified latent representation of the drug–material pair. This combined representation was then passed through a multilayer perceptron (MLP), which performs regression to predict the corresponding adsorption energy. A schematic illustration of the overall model architecture and workflow is provided in Fig. 1 and 2.

2.2.1. Training. The training strategy adopted in this work is based on the transfer learning paradigm, which enhances numerical stability and model generalization, particularly in scenarios with limited data. Initially, a graph convolutional network (GCN) was trained as an encoder, paired with a multilayer perceptron (MLP) decoder, using the large scale QM9 dataset. This pre-training phase allowed the encoder to learn rich molecular representations from a diverse set of drug-like compounds. After completion of this stage, the MLP decoder was discarded, and the encoder was transferred to the new model architecture designed for adsorption energy prediction.

In the second phase, the fine-tuning process was carried out using the drug–material adsorption dataset, which contained only 67 data points. Among them, 5 of the data points contain the results of drug and GrS adsorption energy computed before training the model. These 5 points help tune the model further.

To preserve the learned molecular representations and prevent overfitting, the parameters of the pre-trained encoder were frozen, allowing only the newly added lightweight MLP to be trained on the adsorption data. For both pre-training and fine-tuning phases, the mean squared error (MSE) was employed as the loss function to minimize the deviation between predicted and actual adsorption energies.

Initially, we train the encoder on the QM9 dataset and tune hyperparameters *via* a grid search. The best encoder is chosen based on the validation accuracy. Subsequently, the encoders are frozen and the decoder is trained to predict the adsorption energy. This training is guided by *K*-fold validation to tune hyperparameters. After this, the best hyperparameters are used for inference.

2.3. DFT validation

In this study, we have carried out density functional theory (DFT) simulations using the Vienna *ab initio* Simulation Package (VASP)[35,36] to study the ground state electronic structure of the drug–GrS systems. To describe the interaction between ion cores and valence electrons, the projector augmented wave (PAW) method was utilized, which is widely recognized for its accuracy in electronic structure computations.[37,38] The Perdew–Burke–Ernzerhof (PBE) functional within the generalized gradient approximation (GGA) scheme was employed to account for exchange–correlation interactions.[39] The inclusion of van der Waals interactions is necessary to accurately predict the structural properties. The DFT-D3 method of Grimme with zero-damping function was used to introduce dispersion interactions within the system. The computational parameters are as follows: electronic self-consistency was considered achieved when the energy variation fell below 1.0×10^{-6} eV, while ionic relaxation was deemed converged when the force acting on each ion dropped below 0.001 eV Å^{-1}. Brillouin zone integration was executed using a $10 \times 10 \times 1$ *k*-point grid. Furthermore, the plane-wave energy cutoff was set to 520 eV. In the present study, following standard practice in first-principles surface science, the adsorption energy (E_{ads}) was computed[40–43]

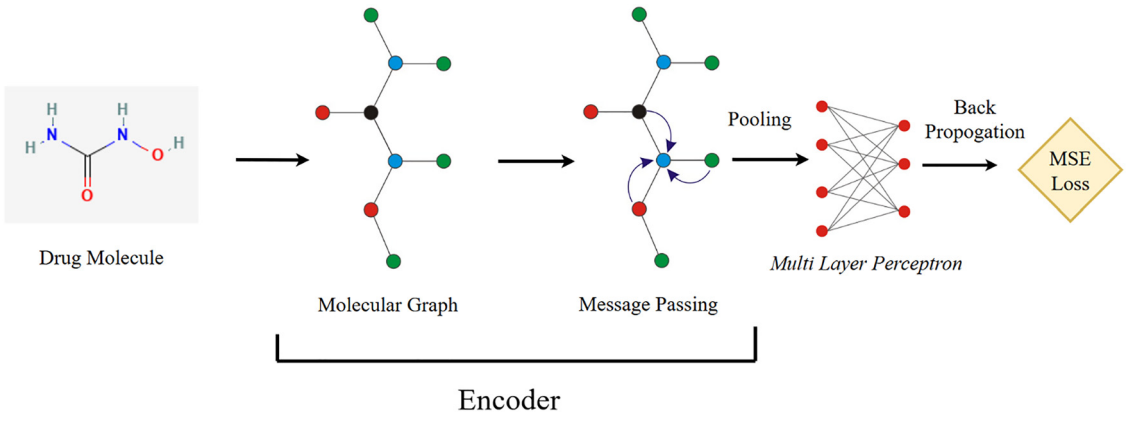

Fig. 1 Encoder training pipeline.

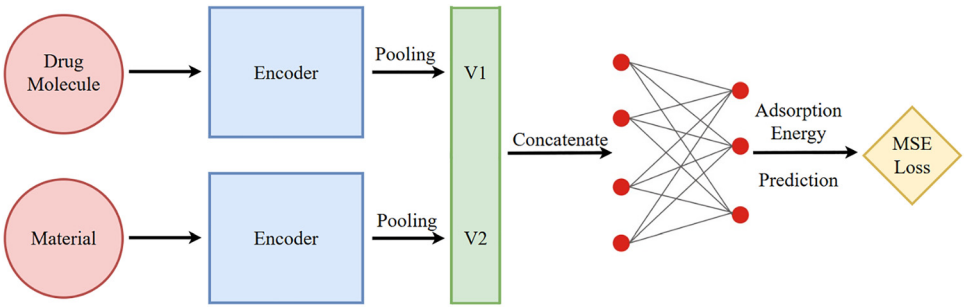

Fig. 2 Complete pipeline.

using the total energies of three separate systems: the clean graphsene substrate, the isolated adsorbate, and the combined adsorbate–substrate system after full relaxation. Specifically, the adsorption energy was evaluated as follows:

$$E_{ads} = E_{drug,graphsene} - E_{graphsene} - E_{drug} \quad (1)$$

where $E_{drug.graphsene}$ is the total energy of the fully relaxed adsorbate–surface complex, $E_{graphsene}$ is the total energy of the relaxed clean surface, and E_{drug} is the total energy of the isolated adsorbate under vacuum. A negative E_{ads} indicates thermodynamically favourable adsorption, with more negative values corresponding to stronger interactions between the drug molecule and the graphsene.

3. Results and discussion

3.1. Structural details of graphsene (GrS)

Fig. 3 presents the optimized atomic structure and charge density distribution of the graphsene (GrS) supercell, as obtained from density functional theory (DFT) calculations. The rectangular supercell is composed of forty carbon atoms, arranged within orthogonal lattice dimensions of a = 10.05 Å and b = 12.78 Å.

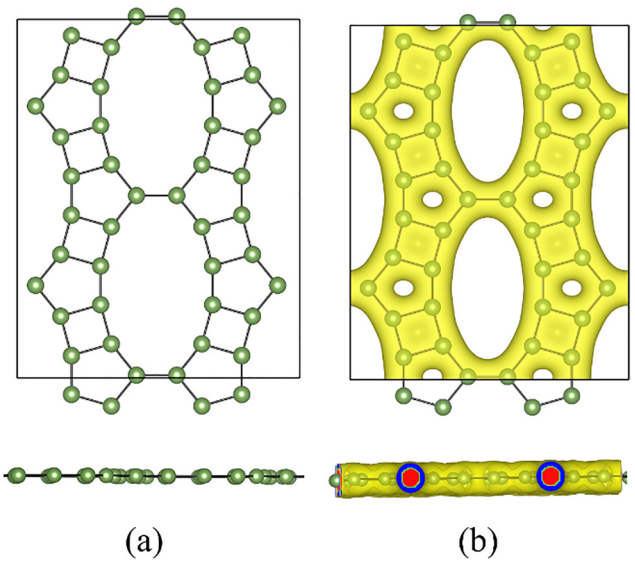

Fig. 3 Top and side views of (a) the optimized GrS supercell and (b) the corresponding charge density distribution.

The fully relaxed geometry exhibits excellent structural stability, and the calculated lattice parameters show strong agreement with previously reported values for related carbon-based monolayers. This consistency confirms that GrS maintains robust mechanical strength and thermodynamic stability, essential for practical applications.

The GrS monolayer displays a complex polygonal ring architecture, incorporating a combination of tetragonal, pentagonal, and dodecagonal carbon rings. This irregular ring topology introduces significant porosity and anisotropy into the lattice, which distinguishes it from conventional graphene. The open channels and large voids within the GrS framework substantially increase the accessible surface area, while the directional variation in bond orientation leads to anisotropic electronic and mechanical behavior. The charge density analysis further reveals a well-distributed electronic cloud throughout the network, indicating strong covalent bonding among carbon atoms and enhanced delocalization of π-electrons, which are favorable for adsorption and charge transfer processes.

This distinctive structural configuration provides several advantages for drug adsorption and delivery applications. The inherent porosity and diverse ring topology create multiple active adsorption sites, enabling strong yet reversible binding of drug molecules through van der Waals, π–π, or electrostatic interactions. Moreover, the high surface to volume ratio of GrS enhances the loading capacity, while its chemical stability and biocompatibility ensure minimal degradation or toxicity under physiological conditions. The combination of these properties makes graphsene an excellent platform for efficient and controllable drug loading and release. Furthermore, its unique electronic characteristics allow for sensitive detection and monitoring of drug–substrate interactions, suggesting that GrS could serve as a multifunctional material for next-generation bio-nanotechnological and therapeutic applications.

3.2. Convergence of the model

In the training phase, the model achieves an $R^2 \approx 0.69$, corresponding to an RMSE of 0.93 against a target standard deviation of 1.67. Thus, the model is statistically significant and suitable for screening. To evaluate the stability and reliability of the machine learning (ML) framework in predicting adsorption energies, a detailed convergence analysis was performed by training and testing the model under multiple random

Table 1 Comparison of ML-predicted and DFT-calculated adsorption energy (E_{add}) between graphsene (GrS) and some selected drug molecules

Drugs and their chemical compositions	Calculated E_{add} (eV)	ML-predicted E_{add} (eV)	ΔE_{add} (eV)
Ifosfamide ($C_7H_{15}Cl_2N_2O_2P$)	−0.566	−0.576	0.010
Pyrazinamide (pyrazinoic acid amide) ($C_5H_5N_3O$)	−0.397	−0.294	0.103
Metformin hydrochloride (glucophage) ($C_4H_{11}N_5{\cdot}HCl$)	−0.943	−1.099	0.157
Zidovudine (Retrovir) ($C_{10}H_{13}N_5O_4$)	−0.365	−0.491	0.126
Captopril (Capoten) ($C_9H_{15}NO_3S$)	−0.615	−0.566	0.049
Tiopronin (Thiola) ($C_5H_9NO_3S$)	−0.388	−0.392	0.004

initialization conditions. Initially, a random seed was selected to generate preliminary adsorption energy predictions for a diverse set of drug molecules. Based on these initial predictions, several drug candidates were shortlisted by considering their molecular size (*i.e.*, the number of constituent atoms), predicted adsorption energy range, and potential pharmaceutical relevance. Subsequently, density functional theory (DFT) calculations were carried out on these selected candidates to validate the ML predictions, and the comparative results are summarized in Table 1. The accuracy of the ML predictions was quantitatively assessed using the mean absolute error (MAE), defined as follows:

$$\mathrm{MAE} = \frac{1}{N}\sum_{i=1}^{N}\left|E_i^{\mathrm{predicted}} - E_i^{\mathrm{DFT}}\right| \quad (2)$$

where $E_i^{\mathrm{predicted}}$ and E_i^{DFT} represent the predicted and reference (DFT calculated) adsorption energies for the ith drug, respectively, and N is the total number of tested molecules. Based on the values predicted in the inference phase and the DFT results, the model achieves an MAE value of 0.075 eV. This demonstrates that the ML model exhibits a high degree of accuracy in approximating DFT calculated adsorption energies, effectively identifying potential drug candidates for further theoretical and experimental validation. However, since neural network based models can be sensitive to random weight initialization, the model's performance may vary slightly with different random seeds. To investigate this effect, the model was trained and evaluated using ten distinct random seeds. The resulting distribution of predicted adsorption energies for each seed is illustrated in Fig. 4, providing a visual comparison of prediction stability. For each seed, the adsorption energies are predicted for all the drugs. Then, we compute the mean and median absolute error against the DFT benchmarks, for each seed. Finally, we assess the distribution of the errors across the seeds to evaluate overall convergence.

The aggregated prediction errors corresponding to each seed are depicted in Fig. 5, which reveals that approximately half of the seed configurations produced predictions within 0.1 eV of the DFT reference values. This level of precision confirms that the ML model consistently captures the underlying energy trends of the system. Nevertheless, a few outlier drugs exhibited anomalously high adsorption energies, which can be attributed to either complex adsorption geometries or limited representation of similar chemical environments in the training dataset.

Therefore, the convergence study confirms that the proposed ML model demonstrates robust predictive capability and numerical stability, with reproducible adsorption energy predictions across multiple initializations. This reliable convergence reinforces its applicability as a pre-screening tool for identifying promising drug and graphsene interaction candidates prior to costly DFT evaluations.

3.3. Structural insights into GrS and drug interactions

Fig. 6 presents the optimized geometries of three representative drug molecules captopril, metformin hydrochloride, and pyrazinamide adsorbed on the graphsene (GrS) monolayer. The corresponding configurations for ifosfamide, zidovudine, and tiopronin molecules are shown in Fig. S1, SI. To provide a deeper understanding of the electronic response upon adsorption, Fig. S2 (SI) illustrates the charge density distributions of all these drug GrS systems from both top and side perspectives,

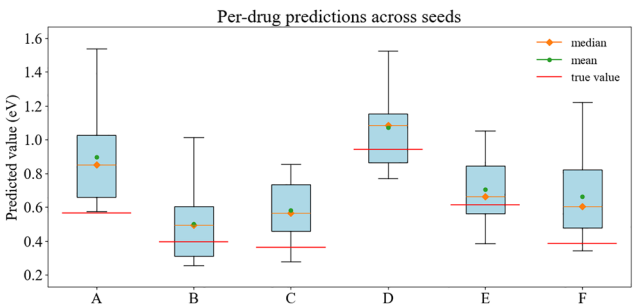

Fig. 4 Box plot: Per-drug prediction distributions across random seeds of (A) GrS + ifosfamide, (B) GrS + pyrazinamide, (C) GrS + zidovudine, (D) GrS + metformin hydrochloride, (E) GrS + captopril, and (F) GrS + tiopronin.

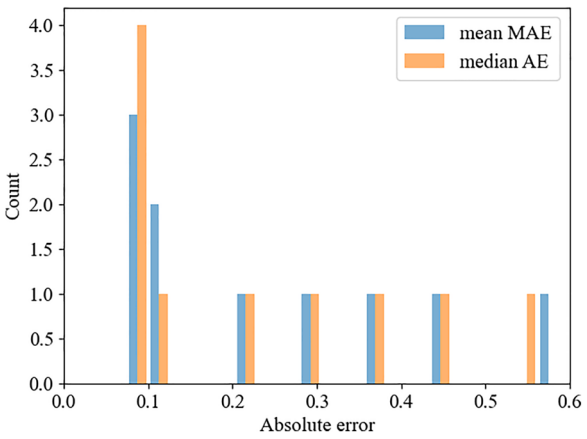

Fig. 5 Mean/median absolute error against seed count.

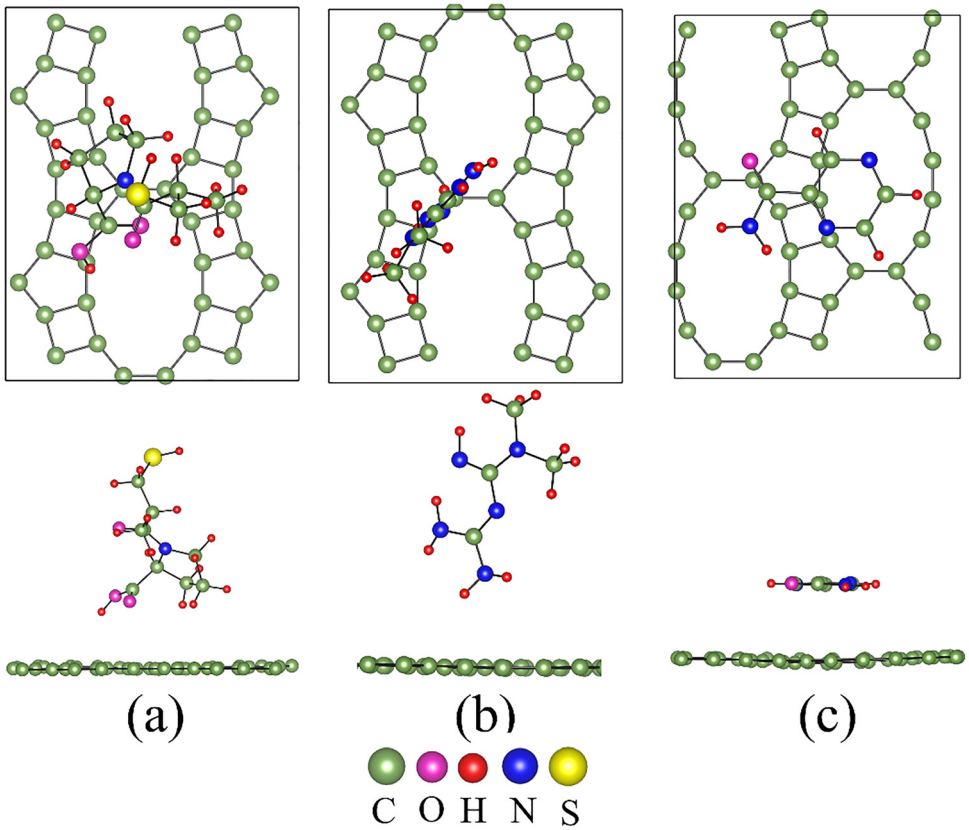

Fig. 6 Top and side views of the optimized structures of GrS with adsorbed (a) captopril, (b) metformin hydrochloride, and (c) pyrazinamide.

while Fig. S3 (SI) displays the isolated structures of the individual drug molecules for reference. From the top view, the characteristic pore-like hexagonal framework of the GrS monolayer is distinctly visible, confirming the structural integrity of the substrate after drug adsorption. Each drug molecule exhibits a unique adsorption orientation and interaction pattern depending on its molecular geometry, size, and functional group composition. Captopril, a sulfur- and oxygen-containing molecule, assumes a nearly upright configuration with its heteroatoms (–SH and –COOH groups) oriented toward the GrS surface, indicating potential localized interactions *via* weak van der Waals forces or hydrogen bonding. In contrast, metformin hydrochloride aligns more parallel to the substrate, suggesting an extended surface contact area that enhances electrostatic and dipole-induced interactions. Pyrazinamide, on the other hand, displays a nearly planar orientation in close proximity to the GrS lattice. This arrangement suggests dominant π–π stacking interactions between the aromatic ring of the drug and the delocalized π-electron network of GrS, leading to a stable adsorption geometry.

The side-view analysis provides further quantitative insights into the adsorption distances and spatial configurations. For captopril, the minimum vertical distance between the molecular backbone and the GrS surface is approximately 2.54 Å, suggesting moderate physisorption accompanied by slight vertical flexibility. Metformin hydrochloride exhibits a slightly larger separation of about 2.66 Å, yet maintains multiple interaction sites across its planar molecular framework. Pyrazinamide, however, shows the most intimate contact with the GrS monolayer, characterized by a minimum adsorption height of 3.38 Å, indicating stronger interfacial coupling primarily driven by π–π interactions. These structural and orientational insights emphasize that the adsorption configuration of each drug molecule on GrS is strongly influenced by its chemical composition and electronic distribution. The variations in the adsorption distance, alignment, and orientation directly affect the degree of electronic coupling between the drug and the substrate. Consequently, these parameters are expected to play a crucial role in modulating charge transfer characteristics, adsorption strength, and the potential efficiency of GrS as a drug delivery carrier, as further analyzed in the subsequent sections on the electronic structure and charge redistribution.

3.4. Partial density of states analysis

Fig. 7 illustrates the partial density of states (PDOS) of pristine GrS and GrS after adsorption of three representative drug molecules: captopril, metformin hydrochloride, and pyrazinamide. The PDOS of pristine GrS exhibits a perfectly symmetric distribution around the Fermi level, with a characteristic vanishing density of states precisely at the Fermi energy (E_F). This feature is consistent with the semi-metallic nature of GrS and reflects the presence of Dirac cones at the *K*-point in its band structure. Such an electronic configuration accounts for the exceptionally high carrier mobility

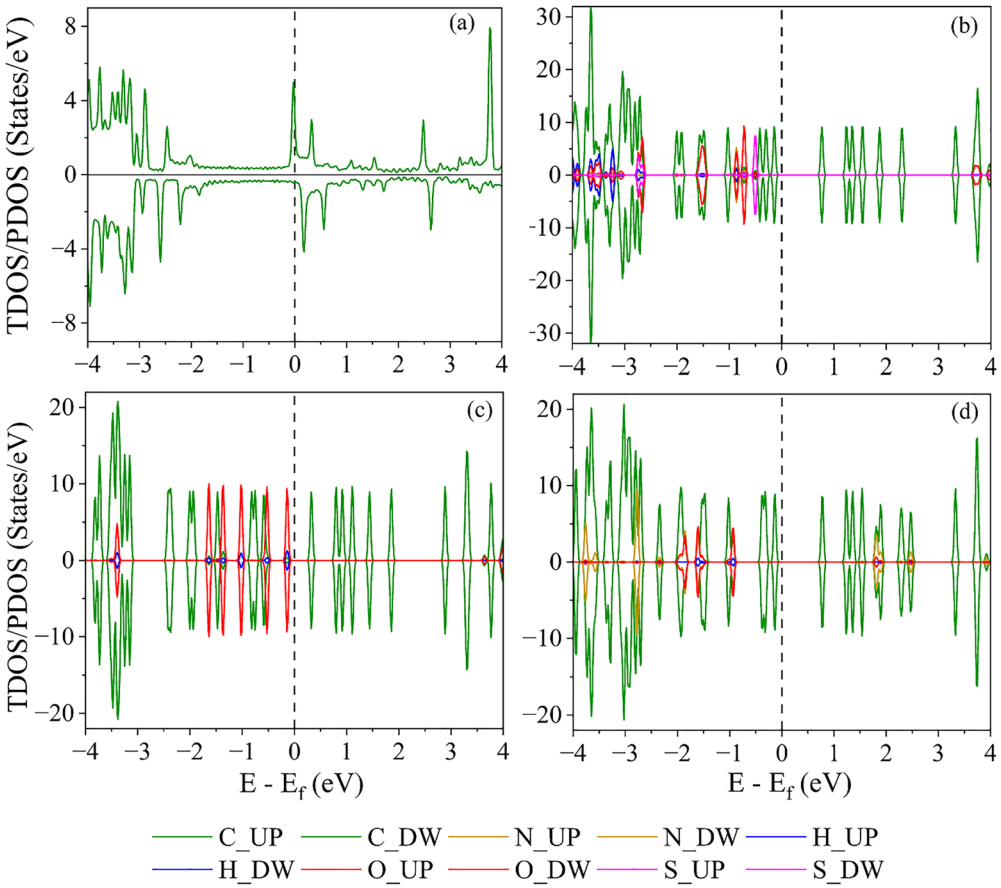

Fig. 7 Projected density of states (PDOS) plots for (a) pristine GrS, (b) GrS + captopril, (c) GrS + metformin hydrochloride and (d) GrS + pyrazinamide.

and intrinsic conductivity observed in pristine GrS, confirming its potential as a highly responsive substrate for adsorption-based applications.

After adsorption of captopril on the GrS surface, the PDOS profile undergoes significant modification. New states emerge near the Fermi level, accompanied by peak broadening and asymmetry. These changes arise from orbital hybridization between the molecular orbitals of captopril and the π states of GrS. Moreover, the presence of finite states around E_F indicates charge transfer between the drug molecule and the GrS sheet, effectively altering the local electronic environment. The formation of such hybridized states suggests a strong electronic interaction, which enhances the chemical reactivity of GrS and improves its sensitivity toward captopril adsorption, an important feature for sensor-based and drug-delivery applications.

In the case of GrS + metformin hydrochloride, distinct alterations in the PDOS are observed across the energy range from approximately −3 eV to +1 eV relative to the Fermi level. Several new states appear in this range, indicating a moderate degree of electronic coupling and partial charge transfer between the drug and the substrate. The overlap between the electronic states of metformin hydrochloride and those of GrS leads to a redistribution of charge density, implying an effective interaction that modifies the local potential landscape. This behavior suggests that metformin hydrochloride forms a relatively stable adsorption complex on GrS, characterized by both physisorption and weak chemisorption contributions.

For the GrS + pyrazinamide complex, the PDOS exhibits additional, though comparatively less intense, features near the Fermi level. While the changes in PDOS magnitude are less pronounced than those observed for captopril and metformin hydrochloride, the emergence of subtle peaks around E_F points to weak electronic coupling and donor acceptor type interactions between pyrazinamide and the GrS sheet. This mild perturbation reflects a weaker adsorption strength, yet it confirms that even small molecules like pyrazinamide can influence the local electronic structure of GrS through Frontier orbital interactions.

So, the PDOS analysis of the pure Grs and GrS + drug systems provides deep insight into the electronic interactions and charge transfer dynamics governing drug adsorption on GrS. The appearance of new electronic states and the redistribution of density near the Fermi level clearly indicate orbital hybridization and charge redistribution between the adsorbates and the substrate. These modifications directly affect the electronic conductivity, surface reactivity, and sensing efficiency of GrS, underscoring its suitability as a multifunctional platform for drug detection and controlled delivery systems.

Table 2 Calculated Bader charge difference (or charge exchange) (Δq in e) between GrS and the adsorbed drug

Systems	Δq in e
GrS + captopril	−0.066
GrS + metformin hydrochloride	0.051
GrS + pyrazinamide	−0.009

3.5. Bader charge analysis

To further elucidate the electronic interactions between the adsorbed drug molecules and the substrate, Bader charge analysis[44] was performed. The charge transfer upon adsorption (Δq) quantifies the redistribution of electron density between the drug and the substrate. Here, a negative Δq value indicates that the drug acts as an electron acceptor (gaining electrons), while a positive value implies electron donation to the substrate. The Bader charge differences calculated for the investigated drug molecules are summarized in Table 2, while the comprehensive dataset is provided in Tables S1 and S2 (SI).

The modifications in the PDOS following drug adsorption are in excellent agreement with the trends observed in the Bader charge analysis. For instance, the substantial emergence of new states near the Fermi level and pronounced peak broadening in the captopril-adsorbed system correlate with the largest negative Bader charge value $\Delta q = -0.066$, confirming significant electron transfer from graphene to the drug. Similarly, the moderate PDOS changes seen for metformin hydrochloride are consistent with its mild electron-donating behavior $\Delta q = 0.051$, while the relatively subtle PDOS alterations in the pyrazinamide system reflect the minimal charge transfer observed, $\Delta q = -0.009$. Together, these results demonstrate that the degree of charge transfer, as quantified by Bader analysis, directly influences the extent of electronic structure modification in graphene upon drug binding. This interplay between orbital hybridization and charge redistribution underpins both the strength and character of the adsorption process, ultimately impacting the material's efficacy in sensing or drug-delivery applications.

4. Conclusion

This study presents a data-driven computational framework that integrates graph neural network (GNN)-based machine learning (ML) predictions with density functional theory (DFT) validation to evaluate drug adsorption on graphsene (GrS) monolayers. By combining predictive screening with quantum-level confirmation, the workflow offers an accelerated and scalable approach for identifying promising drug–substrate interactions within complex chemical spaces.

The ML model demonstrated strong predictive capability with a mean absolute error (MAE) of 0.075 eV, effectively capturing key physicochemical trends across diverse drug molecules. Minor sensitivities to random initialization and certain molecular outliers suggest that expanding the dataset, refining molecular descriptors, and optimizing the network architecture could further improve model robustness. Complementary DFT analyses, including projected density of states (PDOS) and Bader charge studies, revealed hybridized electronic states and charge redistribution near the Fermi level upon adsorption, indicating strong orbital hybridization and charge transfer. Among the examined drugs, captopril showed the strongest electronic coupling, followed by metformin hydrochloride and pyrazinamide, highlighting how the molecular structure influences interaction strength.

Therefore, the integrated ML-DFT framework provides a powerful and interpretable platform for rapid screening and rational design of drug–nanomaterial interfaces. This synergy between AI-driven prediction and first-principles validation underscores a promising route toward accelerating discovery of next-generation nanomaterials for biomedical applications, such as drug delivery, biosensing, and molecular recognition.

Author contributions

Chaithanya Purushottam Bhat contributed primarily to VASP simulations, data analysis, figure preparation, reference management, and manuscript review and revision. Pranav Suryawanshi wrote the draft, trained the ML model, and edited graphical representations. Aditya Guneja was responsible for the literature survey and preparation of the dataset. Debashis Bandyopadhyay, the corresponding author, was responsible for overall project coordination, conceptual design, VASP computations, data interpretation, manuscript drafting and editing, and project administration. These CRediT roles provide a clear and transparent account of each author's contributions to the research.

Conflicts of interest

The authors confirm that they have no financial interests or personal relationships that could be perceived as conflicting with the research presented in this paper.

Data availability

All data are presented in terms of tables, graphs and figures. However, other additional data will be made available on request.

Supplementary information (SI) is available. See DOI: https://doi.org/10.1039/d5ma01519g.

Acknowledgements

The authors gratefully acknowledge the Anusandhan National Research Foundation (ANRF), Government of India, for the research support provided through the grant CRG/2022/003249, which made this work possible. To enhance language quality and ensure proper citation, the authors utilized Grammarly and Turnitin during the manuscript preparation. Following the use of these tools, the authors carefully reviewed and

revised the content as needed and take full responsibility for the accuracy and integrity of the final manuscript.

References

1 D. Peer, J. M. Karp, S. Hong, O. C. Farokhzad, R. Margalit and R. Langer, Nanocarriers as an emerging platform for cancer therapy, *Nat. Nanotechnol.*, 2007, **2**(12), 751–760, DOI: 10.1038/nnano.2007.387.

2 M. L. Etheridge, S. A. Campbell, A. G. Erdman, C. L. Haynes, S. M. Wolf and J. McCullough, The big picture on nanomedicine: The state of investigational and approved nanomedicine products, *Nanomedicine*, 2013, **9**(1), 1–14, DOI: 10.1016/j.nano.2012.05.013.

3 K. S. Novoselov, A. Mishchenko, A. Carvalho and A. H. Castro Neto, 2D materials and van der Waals heterostructures, *Science*, 2016, **353**(6298), aac9439, DOI: 10.1126/science.aac9439.

4 K. AbouAitah, F. Sabbagh and B.-S. Kim, Graphene Oxide Nanostructures as Nanoplatforms for Delivering Natural Therapeutic Agents: Applications in Cancer Treatment, Bacterial Infections, and Bone Regeneration Medicine, *Nanomaterials*, 2023, **13**, 2666, DOI: 10.3390/nano13192666.

5 L. Cheng, X. Wang, F. Gong, T. Liu and Z. Liu, 2D nanomaterials for cancer theranostic applications, *Adv. Mater.*, 2020, **32**(13), 1902333, DOI: 10.1002/ADMA.201902333.

6 L. Ding, M. Liang, C. Li, X. Ji, J. Zhang, W. Xie, R. L. Reis, F.-R. Li, S. Gu and Y. Wang, Design strategies of tumor-targeted delivery systems based on 2D nanomaterials, *Small Methods*, 2022, **6**(10), 2200853, DOI: 10.1002/smtd.202200853.

7 X. Han, J. Huang, H. Lin, Z. Wang, P. Li and Y. Chen, 2D ultrathin MXene-based drug-delivery nanoplatform for synergistic photothermal ablation and chemotherapy of cancer, *Adv. Healthcare Mater.*, 2018, **7**(9), 1701394, DOI: 10.1002/ADHM.201701394.

8 H. Zhang, L. Zhang, Z. Cao, S. Cheong, C. Boyer, Z. Wang, S. L. J. Yun, R. Amal and Z. Gu, Two-dimensional ultra-thin nanosheets with extraordinarily high drug loading and long blood circulation for cancer therapy, *Small*, 2022, **18**(22), 2200299, DOI: 10.1002/smll.202200299.

9 M. Hosseini, M. Soleimani, F. Shojaei and M. Pourfath, Graphsene as a novel porous two-dimensional carbon material for enhanced oxygen reduction electrocatalysis, *Sci. Rep.*, 2024, **14**(1), 9129, DOI: 10.1038/s41598-024-59756-3.

10 N. M. Quan and V. V. Thanh, A molecular dynamics study on mechanical properties of Graphsene, in Proceedings of the 2nd International Conference on Sustainability and Emerging Technologies for Smart Manufacturing, 2025, Springer Nature Singapore, pp. 589–595, DOI: 10.1007/978-981-95-1750-3_67.

11 M. Hosseini, M. Soleimani, F. Shojaei and M. Pourfath, Graphsene: A new porous two-dimensional carbon-based material with anisotropic behavior in electronic and mechanical properties and highly efficient ORR electrocatalytic activity, *Sci. Rep.*, 2024, DOI: 10.21203/rs.3.rs-3939380/v1.

12 D. Belletto, V. Vigna, P. Barretta, F. Ponte, G. Mazzone, S. Scoditti and E. Sicilia, Computational assessment of the use of graphene-based nanosheets as Pt[II] chemotherapeutics delivery systems, *J. Comput. Chem.*, 2024, **45**(24), 2059–2070, DOI: 10.1002/jcc.27394.

13 M. Shahabi and H. Raissi, Screening of the structural, topological, and electronic properties of the functionalized Graphene nanosheets as potential Tegafur anticancer drug carriers using DFT method, *J. Biomol. Struct. Dyn.*, 2018, **36**(10), 2517–2529, DOI: 10.1080/07391102.2017.1360209.

14 M. A. A. Ibrahim, M. H. A. Hamad, A. H. M. Mahmoud, G. A. H. Mekhemer, S. R. M. Sayed, M. Abd Elrahman, P. A. Sidhom, E. Dabbish and T. Shoeib, On the use of graphene nanosheets for drug delivery: A case study of cisplatin and some of its analogs, *Pharmaceutics*, 2023, **15**(6), 1640, DOI: 10.3390/pharmaceutics15061640.

15 Y. Wang, M. C. Sorkun, G. Brocks and S. Er, ML-aided computational screening of 2D materials for photocatalytic water splitting, *J. Phys. Chem. Lett.*, 2024, **15**(18), 4983–4991, DOI: 10.1021/acs.jpclett.4c00425.

16 M. Fronzi, S. A. Tawfik, M. Abu Ghazaleh, O. Isayev, D. A. Winkler, J. G. Shapter and M. J. Ford, High throughput screening of millions of van der Waals heterostructures for superlubricant applications, *Adv. Theory Simul.*, 2020, **3**(11), 2000029, DOI: 10.1002/adts.202000029.

17 S. Bag, M. Konrad, T. Schlöder, P. Friederich and W. Wenzel, Fast generation of machine learning-based force fields for adsorption energies, *J. Chem. Theory Comput.*, 2021, **17**(11), 7195–7202, DOI: 10.1021/acs.jctc.1c00506.

18 Y. Qin, L. Mu, X. Wan, Z. Zong, T. Li, H. Fang and N. Yang, Deep potential for interaction between hydrated Cs[+] and graphene, *Langmuir*, 2025, **41**(18), 11506–11514, DOI: 10.1021/acs.langmuir.5c00508.

19 V. Fung, G. Hu, P. Ganesh and B. G. Sumpter, Machine learned features from density of states for accurate adsorption energy prediction, *Nat. Commun.*, 2021, **12**(1), 88, DOI: 10.1038/s41467-020-20342-6.

20 X. Ma, Z. Li, L. E. K. Achenie and H. Xin, Machine-learning-augmented chemisorption model for CO_2 electroreduction catalyst screening, *J. Phys. Chem. Lett.*, 2015, **6**(18), 3528–3533, DOI: 10.1021/acs.jpclett.5b01660.

21 V. Bhat, P. Sornberger, B. S. S. Pokuri, R. Duke, B. Ganapathysubramanian and C. Risko, Electronic, redox, and optical property prediction of organic π-conjugated molecules through a hierarchy of machine learning approaches, *Chem. Sci.*, 2023, **14**(1), 203–213, DOI: 10.1039/d2sc04676h.

22 G. Montavon, M. Rupp, V. Gobre, A. Vazquez-Mayagoitia, K. Hansen, A. Tkatchenko, K.-R. Müller and O. A. von Lilienfeld, Machine learning of molecular electronic properties in chemical compound space, *New J. Phys.*, 2013, **15**(9), 095003, DOI: 10.1088/1367-2630/15/9/095003.

23 R. Tran, J. Lan, M. Shuaibi, B. M. Wood, S. Goyal, A. Das, J. Heras-Domingo, A. Kolluru, A. Rizvi, N. Shoghi, A. Sriram, Z. Ulissi and C. L. Zitnick, The Open Catalyst 2022 (OC22) dataset and challenges for oxide electrocatalysts, *ACS Catal.*, 2023, **13**(5), 3066–3084, DOI: 10.1021/acscatal.2c05426.

24 Z. Wang, W. Li, S. Wang and X. Wang, The future of catalysis: Applying graph neural networks for intelligent catalyst design, *Wiley Interdiscip. Rev.: Comput. Mol. Sci.*, 2025, e70010, DOI: 10.1002/wcms.70010.
25 V. Venturi, H. L. Parks, Z. Ahmad and V. Viswanathan, Machine learning enabled discovery of application dependent design principles for two-dimensional materials, *Mach. Learn.: Sci. Technol.*, 2020, **1**(3), 035015, DOI: 10.1088/2632-2153/aba002.
26 S. Pablo-García, S. Morandi and R. A. Vargas-Hernández, *et al.*, Fast evaluation of the adsorption energy of organic molecules on metals via graph neural networks, *Nat. Comput. Sci.*, 2023, **3**(5), 433–442, DOI: 10.1038/s43588-023-00437-y.
27 Y. Liu, X. Liu and B. Cao, Graph attention neural networks for mapping materials and molecules beyond short-range interatomic correlations, *J. Phys.: Condens. Matter*, 2024, **36**(21), 215901, DOI: 10.1088/1361-648X/ad2584.
28 J. E. Saal, A. O. Oliynyk and B. Meredig, Machine learning in materials discovery: Confirmed predictions and their underlying approaches, *Annu. Rev. Mater. Res.*, 2020, **50**, 49–69, DOI: 10.1146/annurev-matsci-090319-010954.
29 X. J. Gao, K. Ciura, Y. Ma, A. Mikolajczyk, K. Jagiello, Y. Wan, Y. Gao, J. Zheng, S. Zhong, T. Puzyn and X. Gao, Toward the integration of machine learning and molecular modeling for designing drug delivery nanocarriers, *Adv. Mater.*, 2024, **36**, 2407793, DOI: 10.1002/adma.202407793.
30 Q. Tong, P. Gao, H. Liu, Y. Xie, J. Lv, Y. Wang and J. Zhao, Combining machine learning potential and structure prediction for accelerated materials design and discovery, *J. Phys. Chem. Lett.*, 2020, **11**(20), 8710–8720, DOI: 10.1021/acs.jpclett.0c02357.
31 Y. Jia, X. Hou, Z. Wang and X. Hu, Machine learning boosts the design and discovery of nanomaterials, *ACS Sustainable Chem. Eng.*, 2021, **9**(18), 6130–6147, DOI: 10.1021/acssuschemeng.1c00483.
32 A. Mannodi-Kanakkithodi and M. K. Y. Chan, Computational data-driven materials discovery, *Trends Chem.*, 2021, **3**(2), 79–82, DOI: 10.1016/j.trechm.2020.12.007.
33 R. Ramakrishnan, P. Dral, M. Rupp and O. A. von Lilienfeld, Quantum chemistry structures and properties of 134 kilo molecules, *Sci. Data*, 2014, **1**, 140022, DOI: 10.1038/sdata.2014.22.
34 RDKit, Open-Source Cheminformatics, https://www.rdkit.org/.
35 G. Kresse and J. Hafner, Ab initio molecular dynamics for liquid metals, *Phys. Rev. B: Condens. Matter Mater. Phys.*, 1993, **47**, 558–561, DOI: 10.1103/PhysRevB.47.558.
36 G. Kresse and J. Hafner, Ab initio molecular-dynamics simulation of the liquid-metal-amorphous-semiconductor transition in germanium, *Phys. Rev. B: Condens. Matter Mater. Phys.*, 1994, **49**, 14251–14269, DOI: 10.1103/PhysRevB.49.14251.
37 G. Kresse and J. Furthmüller, Efficiency of ab initio total energy calculations for metals and semiconductors using a plane-wave basis set, *Comput. Mater. Sci.*, 1996, **6**, 15–50, DOI: 10.1016/0927-0256(96)00008-0.
38 P. E. Blöchl, Projector augmented-wave method, *Phys. Rev. B: Condens. Matter Mater. Phys.*, 1994, **50**, 17953–17979, DOI: 10.1103/PhysRevB.50.17953.
39 S. Grimme, Semiempirical GGA-type density functional constructed with a long-range dispersion correction, *J. Comput. Chem.*, 2006, **27**, 1787–1799, DOI: 10.1002/jcc.20495.
40 C. P. Bhat and D. Bandyopadhyay, Exploring reversible hydrogen storage on Ti- decorated novel 2D graphsene: A DFT investigation, *Int. J. Hydrogen Energy*, 2026, **14**, 152967, DOI: 10.1016/j.ijhydene.2025.152967.
41 C. P. Bhat, B. Bandyopadhyay and D. Bandyopadhyay, Unveiling reversible hydrogen storage mechanism on transition metal decorated 2D holey graphyne: A density functional study, *Int. J. Hydrogen Energy*, 2025, **148**, 150044, DOI: 10.1016/j.ijhydene.2025.150044.
42 C. P. Bhat, B. Bandyopadhyay and D. Bandyopadhyay, A Novel 2D-hBNX covalent inorganic framework functionalized with transition metals for enhanced catechol sensing: A density functional investigation, *Surf. Interfaces*, 2025, **67**, 106653, DOI: 10.1016/j.surfin.2025.106653.
43 C. P. Bhat and D. Bandyopadhyay, Insights into the reversible hydrogen storage mechanism of transition metal-decorated Irida-graphene: A DFT study, *Int. J. Hydrogen Energy*, 2025, **137**, 750, DOI: 10.1016/j.ijhydene.2025.05.072.
44 R. F. W. Bader, *Atoms in molecules: A quantum theory*, Clarendon Press, Oxford, 1990, DOI: 10.1093/oso/9780198551683.001.0001.